Recent results on industrial-scale energy storage with Vanadium Redox Flow Battery

Andrea Trovò[1,2], Piergiorgio Alotto[1,2], Monica Giomo[1,2], Federico Moro[1,2], Massimo Guarnieri[1,2]

[1] Department of Industrial Engineering, University of Padua, Italy

[2] Interdepartmental Centre "Giorgio Levi Cases" for Energy Economics and Technology, University of Padua, Italy

Abstract Vanadium Redox Flow Batteries are increasingly being considered as one of the most interesting options for the storage of large quantities of energy due to their unique advantages. Their development and future diffusion largely depend on the research on new materials as well as on the technological development, but also on the availability of appropriate models which allow their realistic simulation in operative conditions. Although an extensive literature on these topics exists for small devices or single cells, very few investigations are reported in the literature concerning the technology, modelling and simulation of large-scale Vanadium Redox Flow Battery systems, built around multi-cell stacks. This paper presents an industrial-sized 9 kW system, its modelling, validation and operation simulation in realistic conditions. In particular, a complete dynamic model is presented, able to simulate the thermal behavior both in standby, i.e. without power and reactant flow, as well as in operating conditions. The proposed model is validated by comparing computed data with experimental measurements.

Keywords Redox Flow Battery, multi-physics model, thermal model, internal losses, shunt currents

Introduction

Vanadium Redox Flow Batteries (VRFBs) are attracting blooming interest for their important attributes such as the independent sizing of power and energy, competitive manufacturing costs, low environmental impact, high durability and high energy efficiency [1]. Moreover, this technology is expected to drive the expansion of sustainable energy systems, being well suited for applications in smart grids, e.g. for load leveling, peak shaving, uninterruptible power supplies (UPS), emergency backup [2] and energy buffer for electric vehicle recharging stations. Extensive research carried out in the last decades has allowed to enhance their performance by developing, testing, and selecting new materials for membranes [3], electrodes [4], and current collectors [5] as well as for improving the cell geometries and architectures [6]. However, these investigations are usually carried out at laboratory level, on single small-size cells with active areas of 5–10 cm^2 or short stacks consisting of a few small cells, which allow testing at relatively low costs.

Future technological development must focus on system scale-up and optimization of large industrial-scale systems capable of performance improvements and competitive costs, which will assure a widespread diffusion [7]. Nevertheless, due to the considerable investments needed for such large experimental facilities, a limited number of them are present worldwide and even less are reported in the scientific literature [8]. A recent authoritative review [9] quotes "… the majority of publications have been restricted to short term studies of small electrodes in the laboratory; very few contributions have considered pilot-scale devices and the effect of cell design, electrode structure, reaction environment and operational conditions on performance.…". The few examples of kW-scale devices reported in the literature include: a system with a 4-kW stack [10], a 10-kW 31-cell 2714-cm^2 experimental stack, that obtained a top current density of 90 mA cm^{-2} [8] and a 15-cell 780-cm^2 stack operated at 160 mA cm^{-2} [11].

In order to investigate the aforementioned objectives, a 9-kW/26-kWh Vanadium Redox Flow Battery was built and is operated at the Energy Storage and Conversion Lab of the University of Padua, dubbed IS-VRFB (Industrial Scale VRFB) [XX]. It presents a stack architecture compatible with industrial production and is instrumented for full testing programs under laboratory-controlled conditions. Investigations regarded charge and discharge cycles as well as polarization curves obtained with fast and slow dynamics, which occur in primary frequency regulation and peak shaving, respectively [12]. In order to enhance the understanding of the behavior of VRFBs, experiments have been complemented with wide activities of numerical modeling and simulations. In fact, these activities are helpful to analyze the cell performance, felt and membranes behavior and solution flow patterns. In addition, they can be used in the search for operational optimization [13], such as thermal control. Operation around room temperature is one of the advantages of VRFBs and is crucial for their industrial exploitation, since it allows avoiding complex and costly thermal control systems. Consistently, thermal management is now emerging as an important issue of VRFBs, as reported in [9] and [14]. Moreover, high solution concentrations provide higher energy density, but they also imply temperature-dependent ion precipitation issues [15]: in fact, these events can occlude the cell flow channels causing major problems during battery operations and during standby periods, when the pumps are turned-off [19]. To avoid this negative side effects, an accurate close-loop control of the solution temperature is required: for example, in the case of 2.5-M vanadium solutions in sulfate-chloride mix [16], the electrolytes temperatures must be kept in the range from –5°C to +50°C, since lower temperatures induce V^{2+} and V^{3+} precipitation [17] and higher temperatures cause precipitation [18]. Few experimental analyses of this kind performed on large stacks have been documented [9]. A first numerical investigation of a full industrial-scale VRFB system, not including a detail analysis of shunt current effect, is reported in [20].

This paper presents a complete, cell-resolved, dynamic thermal model capable of computing the thermal behavior of a real kW-class VRFB stack in any arbitrary operating conditions. It merges partial models for thermal analyses in specific conditions which were previously reported, i.e. in standby conditions [XX] and in load conditions [XX]. The model takes into account all dissipations which occur in

a kW-class VRFB, i.e. entropic heat, ions crossover, crossover side reactions, and shunt current effects. At this aim, a shunt current equivalent circuit is included and the mass and energy balance equations during operating conditions are considered. The model is applied to the IS-VRFB experiment and validated against its experimental data. In order to cope efficiently with all these physical and thermal effects, a new mathematical scheme has been implemented.

The IS-VRFB at the University of Padua

The system is provided with a stack architecture conforming industrial manufacturing standards and is fully instrumented for extensive measurement campaigns (Fig. 1). The IS-VRFB allows examining the performances of industrial scale stacks in defined operating conditions providing a deeper engineering knowledge on this technology with respect to small single cell devices (or short stacks) [20]. The stack consists of 40 cells; each consisting of a Nafion 212 membrane (active area of 30 cm × 20 cm) and two 5.7-mm graphite felt electrodes enclosed between two flat sintered graphite bipolar plates. Vanadium solutions are stored into two tanks, each one with a capacity of 550 L, and are distributed through flow piping, stack manifolds and cell frame channels (Fig 2). The stack is placed over the tanks, which are set side by side. The centrifugal pumps are installed in the back, at low level to ensure easy triggering, while their powering inverters are placed in the frontal electric panel, for easy access. The tanks are hermetically sealed and oxygen is excluded by a nitrogen filling system. Charge and discharge are provided by a power management system (PMS), which consists of a two-quadrant static converter with local and remote control. The rating of the PMS is ±75 A, 85 V and it is flanked by a passive load consisting of six paralleled variable resistors for testing at high discharge currents, up to 600 A. The in-house battery management system (BMS) guarantees highly versatile measurement management and experimental control. The BMS offers a flexible control according to the requirements of the experimental program and is also suitable for exploring grid-oriented services. The plant is instrumented with electrical, thermal and fluid-dynamic sensors and a multichannel electrochemical impedance spectroscopy (EIS). A surveillance device built around a reliable programmable logic controller (PLC) monitors some measurements and status signals (e.g., inverters, piping valves signals and PMS settings) to ensure high operation safety, flanking some BMS controls on a redundancy concept. The test facility was originally designed for a rated current of 72 A and a rated power of 4 kW. However, after facility upgrade and operation optimization, much higher values of current and power were achieved: 350 A and 8 kW in slow operation (i.e. on timescales over 40 s, which are of interest in energy management grid services) and 400 A and 9 kW in fast operation (i.e. on timescales of 5-20 s, which are of interest in power quality grid services), as shown in Fig. 3 [12]. In fact, in the design stage, rating was based on recent scientific literature data, indicating a current density of 120 mA cm^{-2}, and the performance of the original treatment of the porous electrodes had not yet been checked on large scale. The “present performance data”, reported in Tab.1,

represent the top values actually achieved in the experimental campaign and do not represent the real stack limiting current, available at zero cell voltage.

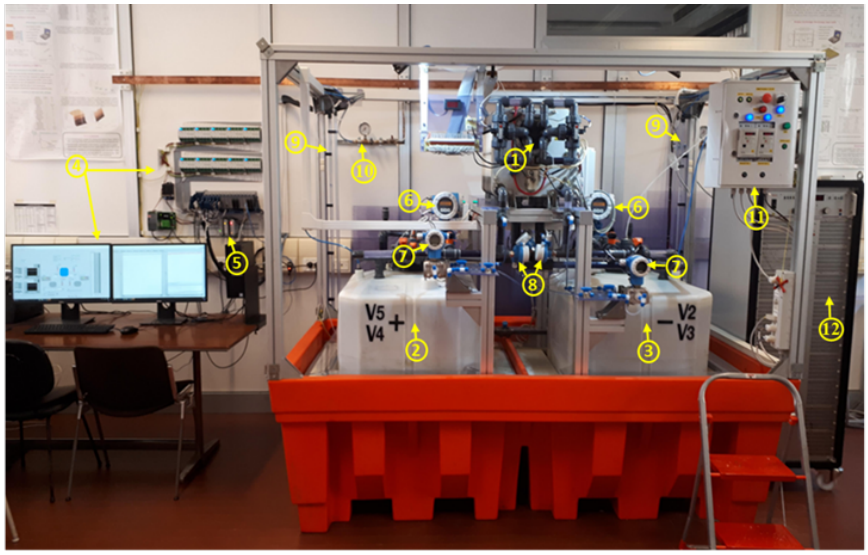

1- Stack
2- Positive electrolyte tank
3- Negative electrolyte tank
4- Labview-based acquisition and management system
5- External PLC
6- Flowmeter
7- Differential pressure transmitter
8- Thermo-resistance
9- Special differential pressure gauge
10- Nitrogen line
11- Electric power board
12- Stack power supply

Fig. 1. The IS-VRFB test facility and its main components.

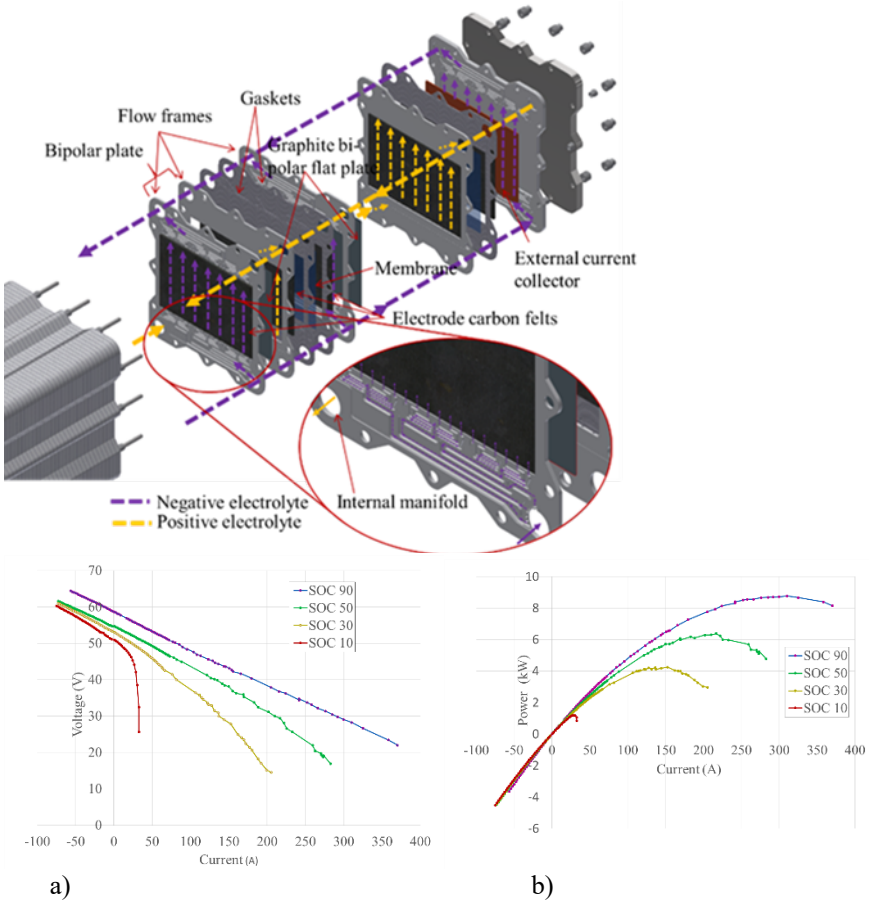

Fig. 3. a) Transient Polarization; b) power curves at various *SOC* values and flow rate of 29.5 L min^{-1}.

Fig. 2. Representation of the IS-VRFB stack

Tab. 1 IS-VRFB test facility features.

Design parameters	
Number of cells	40
Cell active area	30 × 20 cm^2
Tank volume	2 × 550 L
Sulfuric acid concentration	4.5 M
Vanadium concentration	1.6 M
Present performance	
Stored energy	26 kWh
Stack OCV at *SOC*=10%,50%,90%	50.3 V, 54.8 V, 59.3 V
Top current at *SOC*=90%	400 A
Residual voltage at top current and *SOC*=90%	18.5 V
Top power at *SOC*=90%	9 kW
Top current density at *SOC*=90%	665 mA cm^{-2}
Top cell power density at *SOC*=90%	370 mW cm^{-2}

Experimental results

1.1. Polarization curves

Fig. 3 shows the polarization and power curves both in charge and discharge at the following state of charge (*SOC*): 10%, 30%, 50%, 70 % and 90%. During experiments, the solution temperature remained always between 20 °C and 28 °C. Each data point results is the average of some tens of measurements sampled between 5 s and 20 s after starting the stack current. 5 s is the low-end limit to minimize the effect of the initial overcurrent appearing at current start-up, before concentration gradients stabilize inside the electrodes. The upper limit (20 s) was set to limit *SOC* fluctuations during the tests. In the curves of Fig. 3, the points below 75 A were obtained with the bidirectional PMS in both charge and discharge mode. In order to obtain discharge currents higher than 75 A, the passive load

consisting of variable resistors was used. The data at currents between 75 A and 400 A show that the maximum output power in discharge reached 8.9 kW, a value far above the design rated power value of 4 kW. The weight of the stack filled with electrolytic solutions is 115 kg, thus resulting in a stack specific power density of 77 kW kg^{-1}. As shown in Fig. 3, polarization curves present linear trends at high *SOCs*; with an average cell voltage above 0.5 V at 380 A, namely at 635 mA cm^{-2}, when the outpower reaches 8 kW. These results constitute a quite good performance with respect to other 40-cell stack with active cross-sectional areas as large as 600 cm^2 [21]. After early test campaigns, an improvement was implemented consisting in the installation of more powerful pumps, suitable to carry out tests at currents higher than 400 A, in order to approach the limiting currents (i.e. at zero cell voltage). Round Trip Efficiencies (RTEs) measured at 30 A and 70 A current were 71% and 62.5%, respectively [22]. In this case the tests were conducted at constant current, constant flow factor α=8 and charging and discharging the solutions between *SOC* 10% and 90% [23]. The flow factor α is the ratio between the flow rate of the charges transferred by the electrolytes and the electric current generated in the stack by the electrochemical reactions.

Thermal model

The thermal dynamic model considers the entropic heat of the main reactions, the heat generated by the self-discharge reactions associated with the vanadium ions crossover, and the contribution of Joule losses due to the shunt currents. The energy and mass balance equations have been coupled with the equations of the shunt-current circuit, which allow to compute the Joule losses and the heat generated by the pertinent self-discharge reactions. These effects are resolved at the cell level, taking into account the thermal interactions between stack and external components as well as between cells. A detailed description of the model assumptions, governing equations, boundary conditions, and model parameters is reported in [24].

1.2. Redox process and self-discharge reactions

The following simplified set of electrochemical reactions has been considered for the positive and the negative electrodes:

(1)

(2)

Due to the diffusion of vanadium ions across the membrane, exothermic side reactions occur, which cause self-discharge. and move from the negative to the positive compartment and react with and [14], [25], as given by the following reactions:

(3)

(4)

(5)

In the same way, and diffuse towards the negative compartment, reacting with and , according to:

(6)

(7)

(8)

The self-discharge reactions (3) and (4) and (6) and (7), which respectively involve the charged species and , prevail as long as is present in the positive compartment and in the negative one.

1.3. Stack electric model

The stack has been modeled as a lumped electric circuit, see Fig. 6c in [26]. Each cell is represented as a Thévenin equivalent consisting of a voltage source in series with a resistor where $n = 1…40$ is the cell index. These values were experimentally measured, in different operating conditions, i.e. different *SOC*, as reported in [12]. The term corresponds to the cell open circuit voltage (*OCV*) and is obtained using the simplified Nernst equation expressed in terms of *SOC*:

(9)

where is a standard potential that accounts for side effects, $K = 8.314$ J K^{-1}mol^{-1} is the universal gas constant and $F = 96485$ C mol^{-1} is the Faraday constant.
Electrolyte flow paths have been modeled as resistors having resistance:

++ (10)

In eq. (10), l and A are the length and the cross area of the generic element, respectively; $k = m$ for manifold and $k = f$ for flow channel; + and ─ denote the positive and negative electrolytes and compartments, respectively. In particular, σ is computed from the conductivities and concentrations (i.e. *SOCs*) of vanadium ions, according to the flowing equations:

(11)

(12)

where the SOC_- is the ratio between the amount of and the total amount of and while SOC_+ is the ration between the amount of and the total amount of and . The term R_m , represents the resistance between two consecutive cells while R_f is the resistance of the flow channels consisting of a flow frame feeding the cell itself and the cell porous electrode. Positive and negative compartments have the same geometry and R_f is computed by using COMSOL® code. At this aim Fig.4 shows the distribution of the electrical potential when a given shunt current $I_f = 1$A flows for a fixed *SOC*.

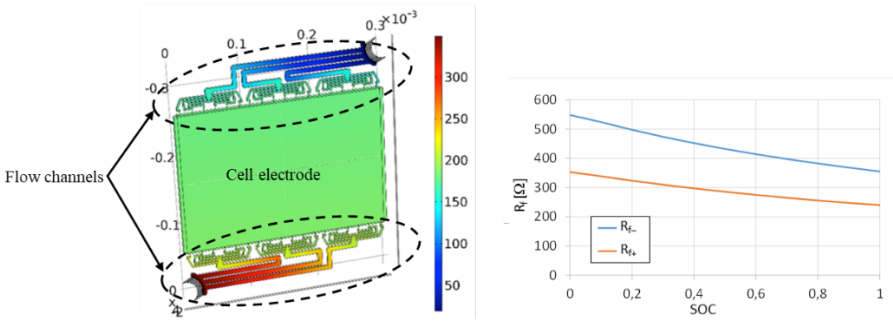

a) b)

Fig.4 a) Electric potential in V where 1-A shunt current flows, the computational domain consisted of porous electrodes (with conductivity σ_e and porosity ϵ) and the flow channels feeding the electrodes.; b) resulting $R_{f+,n}$, $R_{f-,n}$ as functions of *SOC*.

Shunt current losses have been computed by multiplying the shunt currents I by shunt voltages v in each element of the equivalent network.

(13)

(14)

(15)

Further details on the electric model of the IS-VRFB stack are given in [24] and [26].

1.4. Mass and energy balance equations

Single cell mass balances for vanadium ions have been formulated considering the self-discharge processes described by eqs. (3)-(8) and the effects of shunt currents [24]. By modeling the species crossover through the membrane, the mass balance equations during charge/discharge for the negative compartment are written as:

(16)

(17)

(18)

Similar equations result for the positive compartment:

(19)

(20)

(21)

In the case of standby, the mass and energy balance equations differ from (16)-(21) and take into account that the evolution develops in three distinct steps, as reported

in [24]. In both cases the rate of diffusion of each species through the membrane has been evaluated by Fick's law. The diffusivity coefficients, as functions of temperatures, are given in Arrhenius form as:

(22)

where is the diffusivity coefficient of *V(j)* in the *n*-th membrane, k_j is the reference value for *V(j)* and =17340 J mol^{-1} is the activation energy.

The energy balance equation allows to compute the *n*-th cell temperature evolution, T_n:

(23)

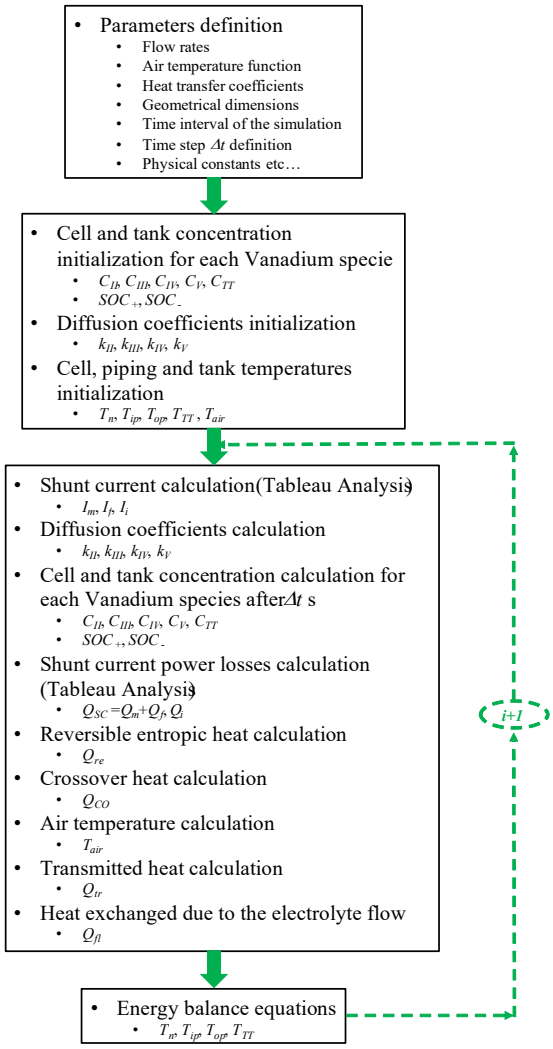

Fig. 5. Thermal model algorithm for charge/discharge operation.

where ρ, C_P and V_C are the density, specific heat at constant pressure of the electrolyte and the cell volume, respectively. This equation includes the following heat contributions: Q_{CO} represents the heat rate generated by the crossover side reactions (3), (4), (6) and (7);

(24)

where ΔH_2, ΔH_3, ΔH_4, ΔH_5, are the enthalpy of reactions (3), (4), (6), (7) respectively. Q_{SC} is the irreversible heat rate produced by the shunt currents in the manifold (R_m) and flow channels (R_f), computed as described in Section 4.2; Q_i is the irreversible heat due to the internal cell overpotential (i.e. due to the internal resistance R_i), Q_{re} refers to the heat rate generated inside the cells by the reactions (1) and (2) supplying the shunt currents:

(25)

Q_{tr} is the transmitted heat rate:

(26)

where U is the heat transfer coefficient of the areas A along the x, y, z, direction [24] and Q_{fl} represents the heat exchange due to the electrolyte flow in each cell that is zero in the standby case:

(27)

1.5. Thermal model implementation

Fig. 5 shows the flow-chart of the overall algorithm for the solution of mass and energy balance equations in the cases of charging/discharging operations. The same algorithm was used to simulate the stand-by evolution, which is based on similar equations, as reported in [24].

At the beginning of the simulation the parameters which define the conditions of the simulation in terms of thermal-fluid dynamic characteristics are set. In this phase the time interval and the time step (Δt) are also defined. In a standard VRFB device, the thermal evolution can be accurately evaluated with Δt =5 s due to the rather slow kinetics of the heat exchange from the stack and piping to the environment. Conversely, after ion crossover, the self-discharge side reactions (3), (4), (5) and (6), (7), (8) are considered instantaneous in each step (i-th iteration on the flowchart Fig.5). In addition, for each cell the perfect mixing of the solution is a reasonable assumption in each compartment, i.e. ions concentrations and temperature are uniform in each cell (such as in a continuous stirred tank reactor, CSTR), as suggested in [27]. After the initialization of the vectors and variables, a simple iterative cycle allows to solve the mass balance equations in order to calculate the concentration variations for each Vanadium species in each cell and from them the heat flux Q_{CO}. In addition, for each iteration, the shunt currents are calculated resorting to the well-known Tableau Analysis technique, which solves the electrical problem, i.e. currents and voltages, associated with the lumped circuit representation of the stack [26]. In such way the overall shunt current losses Q_{SC} and Q_i and reversible entropic heat flux Q_{re} are computed. Similarly, Q_{tr} and Q_{fl} are computed starting from the computed temperature at the (i–1)-th iteration and the energy balance equations (final part of the flowchart in Fig.5) provide the dynamic temperature evolution for each cell at the i-th iteration.

The model has been implemented in Matlab® (MathWorks) and run on a Dell Workstation with 2 Intel® Xeon® processors and 32 GB RAM 2,10 GHz clock.

1.6. Thermal model validation

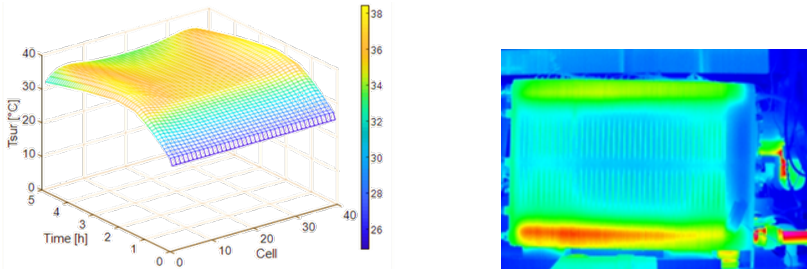

a) b)

Fig. 6. Validation of the stack thermal model during standby by comparison of a) computed lateral superficial temperatures with b) measurements after 1 h from a thermal imager in the IS-VRFB with initial *SOC* = 0.8.

In standby conditions, i.e. with the pumps turned off, the model was validated against experimental data of the lateral surface temperature on the IS-VRFB stack, solved in space and time, taken with a thermal imager (Jade 3 MWIR by CEDIP) at a thermal resolution ±2°C with a space resolution of 320×240 pixels. The validation test was carried considering an initial value *SOC* = 0.8 for the solutions in the stack Fig.6a) shows the cell simulated surface temperatures obtained by the model, whereas thermal measurements provided by the thermal imager are reported in Fig 6b). The simulation results agree well with the temperatures measured after 1 h on the horizontal middle line of the stack, confirming that the coldest cells are in the stack center and the hottest are close to the stack ends. It must be noted the validation confirmed the same accuracy also on the longer standby timescales, as reported in [XX]. As regards the validation of the dynamic thermal model in discharge and charge conditions, numerical results were compared with the temperatures measured by four Pt-100 sensors of the IS-VRFB (T1, T2, T3, T4), together with the air temperature measured by a Pt-100 sensor, which have an accuracy of (±0.15+0.002T)°C. T1 and T3 are the inlet temperatures of the positive and the negative electrolyte respectively and T2 and T4 the outlet temperatures of the positive and the negative side, respectively. The evolution of the positive and negative electrolyte temperatures in charging condition are plotted in Fig.7 a and b, respectively. The thermal model can give a good prediction of the electrolyte temperatures during charging. In fact, simulated and measured temperatures show a maximum discrepancy of 0.9°C, that can be attributed to the assumed simplifications and to the uncertainty of some heat transfer coefficients taken from the literature [28]. The discharging test was performed as well, with a good agreement between numerical and experimental results. Therefore, the thermal model can provide a reliable prediction of the electrolyte temperature evolution in both charge and discharge [29].

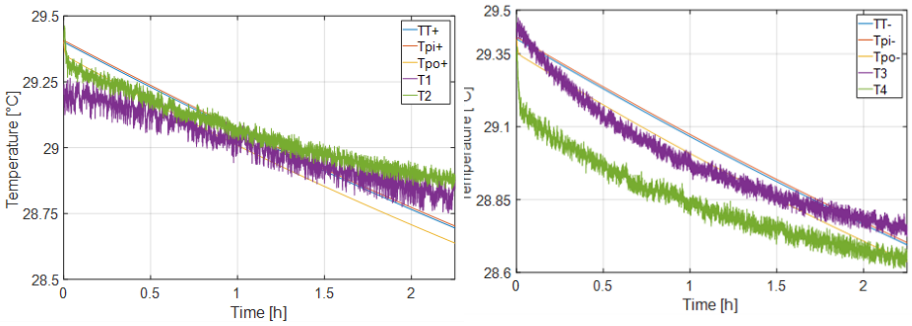

a) b)

Fig. 7. Stack inlet and outlet temperature at the positive side (a) and at the negative side (b) during charging.

Conclusions

A test facility for industrial-sized VRFBs, named IS-VRFB, has been recently completed and put into operation at the University of Padua, Italy. In order to simulate its behavior under realistic conditions, i.e. both during standby and in charge/discharge, a complete dynamic thermal model has been developed. The model takes into account all main physically relevant phenomena, including main electrochemical reactions, ions crossover through the membranes, the inherent self-discharge effects and shunt currents losses. In order to couple all these effects, a specific numerical formulation was developed. The model was successfully validated against experimental data collected from the IS-VRFB test facility in both cases. The model provides the thermal evolution of a VRFB stack resolved at cell level: it has allowed to identify the most critical dissipative effects and can thus be used to guide the design of new thermally optimized systems. In addition, for a given VRFB system, it allows to identify which operating conditions can be critical from the thermal point of view. To our knowledge, this is the first numerical model capable of taking into account also the effect of shunt currents in computing the temperature evolution among the cells in the stack over time, in a kW-class VRFB.

Acknowledgements

This work was funded by the University of Padua under the strategic project MAESTRA 2011 “From Materials for Membrane-Electrode Assemblies to Electric Energy Conversion and Storage Device” (cod. STPD11XNRY 002) and the Project 2016 of the Interdepartmental Centre Giorgio Levi Cases for Energy Economics and Technology (GUAR_RICERCALASCITOLEVI17_02).

Nomenclature

Full symbols	
A	membrane active area
A_k	cross-sectional area in the k-th direction/of k-th element
C	vanadium specie concentration
C_p	electrolyte specific heat at constant pressure
d	membrane thickness
E'_o	corrected standard reversible potential
E_a	activation energy of diffusivity coefficients
E_o	reversible potential – OCV
F	Faraday constant = 96 485 C mol^{-1}
H	enthalpy
I	electric current
k	diffusivity coefficient
K	universal gas constant = 8.314 J $K^{-1}mol^{-1}$
l	length of resistive segment
N	number of cells
OCV	open circuit voltage
P	power
Q	heat
q	flow rate
R	resistance
S	entropy
SOC	state of charge
t	time
T	temperature
U	heat transfer coefficient
v	electric voltage
V_C	cell volume
$V(j)$	j-th vanadium ions
ϵ	carbon felt porosity
ρ	electrolyte density
σ	electrical conductivity
Subscript	
–	negative solution and electrode
+	positive solution and electrode
air	*air*
c	cell
e	electrode
f	flow cannels
fl	heat exchange due to the electrolyte flow
re	cell entropic heat released in energizing shunt current
CO	crossover
i	internal
m	manifold
n	*n-th* cell
pi	piping at the stack inlet
po	piping at the stack outlet
re	cell entropic heat released in energizing shunt current
SC	shunt current

tr	transmitted
TT	tank
V(j)	*j*-th vanadium specie

References

[1] Alotto P, Guarnieri M, Moro F. Redox flow batteries for the storage of renewable energy: A review. Renew Sustain Energy Rev 2014. 22: 59-67: doi:10.1016/j.rser.2013.08.001.

[2] Shah AA, Walsh FC. Electrochimica Acta Non-isothermal modelling of the all-vanadium redox flow battery. Electrochim Acta 2009;55:78–89. doi:10.1016/j.electacta.2009.08.009.

[3] Zhou XL, Zhao TS, An L, Zeng YK, Zhu XB. Performance of a vanadium redox flow battery with a VANADion membrane. Appl Energy 2016;180:353–359. doi:10.1016/j.apenergy.2016.08.001.

[4] Maggiolo D, Zanini F, Picano F, Trovò A, Carmignato S, Guarnieri M. Particle based method and X-ray computed tomography for pore-scale flow characterization in VRFB electrodes. Energy Storage Materials 2019; 16: 91-96, doi: 10.1016/j.ensm.2018.04.021.

[5] Darling RM, Perry ML. The Influence of Electrode and Channel Configurations on Flow Battery Performance. J Electrochem Soc 2014; 161:A1381–7. doi:10.1149/2.0941409jes.

[6] Messaggi M, Canzi P, Mereu R, Baricci A, Inzoli F, Casalegno A, Zago M. Analysis of flow field design on vanadium redox flow battery performance: Development of 3D computational fluid dynamic model and experimental validation. Appl Energy 2018. 228: 1057-1070 doi:10.1016/j.apenergy.2018.06.148.

[7] Oh K, Yoo H, Ko J, Won S, Ju H. Three-dimensional, transient, nonisothermal model of all-vanadium redox flow batteries. Energy 2015 ;81:3–14. doi:10.1016/j.energy.2014.05.020.

[8] Park DJ, Jeon KS, Ryu CH, Hwang GJ. Performance of the all-vanadium redox flow battery stack. J Ind Eng Chem 2017. Volume 45: 387-390; doi:10.1016/j.jiec.2016.10.007.

[9] Arenas LF, Ponce de León C, Walsh FC. Engineering aspects of the design, construction and performance of modular redox flow batteries for energy storage. J Energy Storage 2017. 11: 119-153 doi:10.1016/j.est.2017.02.007.

[10] Fraunhofer Institute of Chemical Technology ICT. Redox Flow Battery. Available<https://www.ict.fraunhofer.de/en/comp/ae/rfb.html>[retrieved on 20/03/2018].

[11] Kim S, Thomsen E, Xia G, Nie Z, Bao J, Recknagle K, et al. 1 kW/1 kWh advanced vanadium redox flow battery utilizing mixed acid electrolytes. J Power Sources 2013; 237:300–9. doi:10.1016/j.jpowsour.2013.02.045.

[12] Guarnieri M, Trovò A, Marini G, Sutto A, Alotto P. High current polarization tests on a 9 kW vanadium redox flow battery J Power Sources 2019; 431: 239-249; doi.org/10.1016/j.jpowsour.2019.05.035.

[13] Xiong B, Zhao J, Tseng KJ, Skyllas-Kazacos M, Lim TM, Zhang Y. Thermal hydraulic behavior and efficiency analysis of an all-vanadium redox flow battery. J Power Sources 2013; 242:314–24. doi:10.1016/j.jpowsour.2013.05.092.

[14] Yan Y, Li Y, Skyllas-Kazacos M, Bao J. Modelling and simulation of thermal behaviour of vanadium redox flow battery. J Power Sources 2016. 322: 116-128; doi:10.1016/j.jpowsour.2016.05.011.

[15] Kim D, Jeon J. A high-temperature tolerance solution for positive electrolyte of vanadium redox flow batteries. J Electroanal Chem 2017. 801, 92-97 doi:10.1016/j.jelechem.2017.07.037.

[16] Li L, Kim S, Wang W, Vijayakumar M, Nie Z, Chen B, et al. A stable vanadium redox-flow battery with high energy density for large-scale energy storage. Adv Energy Mater 2011. 1: 394–400; doi:10.1002/aenm.201100008.

[17] Wang K, Zhang Y, Liu L, Xi J, Wu Z, Qiu X. Broad temperature adaptability of vanadium redox flow battery-Part 3: The effects of total vanadium concentration and sulfuric acid concentration. Electrochim Acta 2018 ;259:11–9. doi:10.1016/j.electacta.2017.10.148.

[18] M. Skyllas-Kazacos, C. Menictas MK. Thermal stability of concentrated V(V) electrolytes in the vanadium redox cell. J Electrochem Soc 1996; 143:L86. doi:10.1149/1.1836609.
[19] Kazacos M, Cheng M, Skyllas-Kazacos M. Vanadium redox cell electrolyte optimization studies. J Appl Electrochem 1990. 20(3), 463–467 doi:10.1007/BF01076057.
[20] Tang A, McCann J, Bao J, Skyllas-Kazacos M. Investigation of the effect of shunt current on battery efficiency and stack temperature in vanadium redox flow battery. J Power Sources 2013;242: 349–56. doi:10.1016/j.jpowsour.2013.05.079.
[21] Guarnieri M, Trovò A, D'Anzi A, Alotto P, Developing vanadium redox flow technology on a 9-kW 26-kWh industrial scale test facility: design review and early experiments, Appl. Energy 230 (2018) 1425–1434. doi.org/10.1016/j,. apenergy.2018.09.021.
[22] Trovò A, Picano F, Guarnieri M. Comparison of energy losses in a 9 kW vanadium redox flow battery. J Power Sources 2019;440: 227144; doi.org/10.1016/j.jpowsour.2019.227144.
[23] Trovò A, Picano F, Guarnieri M. Maximizing Vanadium Redox Flow Battery Efficiency: Strategies of Flow Rate Control. IEEE Int. Symp. Ind Electron 2019, 8781152: 1977-1982; doi: 10.1109/ISIE.2019.8781152.
[24] A. Trovò, G. Marini, G. Sutto, P. Alotto, M. Giomo, F. Moro, M. Guarnieri, Standby thermal model of a vanadium redox flow battery stack with crossover and shunt-current effects, Appl. Energy 240 (2019) 893–906, doi.org/10.1016/ j.apenergy.2019.02.067.
[25] Li Y, Skyllas-Kazacos M, Bao J. A dynamic plug flow reactor model for a vanadium redox flow battery cell. J Power Sources 2016; 311:57–67. doi:10.1016/j.jpowsour.2016.02.018.
[26] Moro F, Trovò A, Bortolin S, Del Col D, Guarnieri M. An alternative low-loss stack topology for vanadium redox flow battery: Comparative assessment. J Power Sources 2017; 340:229–41. doi:10.1016/j.jpowsour.2016.11.042.
[27] Al-Fetlawi H, Shah A, Walsh F. Non-isothermal modelling of the all vanadium redox flow battery. Electrochim Acta 2009; 55: 78-89; https://doi.org/10.1016/j.electacta.2009.08.009.
[28] Holman JP. Heat transfer. tenth Ed McGraw-Hill Higher Education; 2010.
[29] Trovò A, Saccardo A, Giomo M, Guarnieri M. Thermal modeling of industrial-scale vanadium redox flow batteries in high-current operations. J Power Sources 2019; 424: 204-214.doi.org/10.1016/j.jpowsour.2019.03.080.